MOVING BOUNDARY HEAT EXCHANGER MODEL AND VALIDATION PROCEDURE

Manuel Gräber[1], Nils Christian Strupp[1], Wilhelm Tegethoff[1]

[1]TU Braunschweig, Inst. f. Thermodynamik,
Hans-Sommer-Str. 5, 38106 Braunschweig, Germany

m.graeber@tu-bs.de(Manuel Gräber)

Abstract

A moving-boundary model for condenser and evaporator heat exchangers in vapour compression cycles is presented. The model is formulated as system of differential and algebraic equations suitable for an implementation in the modeling language Modelica. The main idea of moving boundary models is to introduce separate control volumes for two-phase and single phase fluid flow. The boundaries of these control volumes or zones change dynamically. The model consists of a maximum of three zones: superheating, subcooling and condensing/evaporating. During simulation the number of zones dynamically changes by switching between different equations. Occurring discontinuities are formulated in a way that allows the simulation tool to handle them numerically stable. The models are well-suited for control design purposes as well as for model based control. Additionally, a validation procedure is presented. The zone lengths, which are differential states of the model, are measured directly by infrared thermography. This method allows a direct comparison of simulated and measured values of all state variables.

Keywords: Moving Boundary, evaporator, condenser, vapour compression, heat pump.

Presenting Author's Biography

Manuel Gräber studied mechanical engineering at RWTH Aachen with focus on energy technology and numerical simulation. Currently he is research assistant at the Institute for Thermodynamics at TU Braunschweig. His research topics are object-oriented modeling and Nonlinear Model Predictive Control of thermodynamic system. He is member of the Modelica Association, which is a non-profit organization developing the open modeling language Modelica and the Modelica Standard Library.

1 Introduction

Vapour compression cycles for air-conditioning or refrigeration have significant impact on the worldwide primary energy demand. Basically there are two topics where numerical simulation can help to further increase its efficiency: one is design and the other topic is control of such systems. For control topics dynamic system models can be used to test the performance of certain controllers or even as online implementation on the controller for advanced model based control. In all cases heat-exchanger models are a key component of the system model.

The most general equations to describe fluid flow are dynamic partial differential equations (PDE) which describe the conservation of mass, momentum and energy. For simulation on system level the numerical solution of these PDE is way too computationally expensive. There exist different mathematical methods to discretize the spatial dimension of the PDE and transform it into a system of differential and algebraic equations (DAE). The Finite Volume method integrates the PDE over constant volumes. For two-phase flows there is a discontinuity in the fluid property equations when leaving or entering the two-phase zone. The Moving Boundary method takes this explicitly into account. Similar to the Finite Volume method the PDE are integrated over a control volume. But the boundaries of the control volumes are not constant, they are exactly at the points, where the fluid changes from one-phase to two-phase and vice-versa (see Fig. 1). As these points vary with time, the control volumes have moving boundaries.

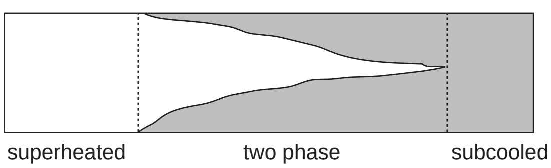

Fig. 1 *Divison of refrigerant flow into three zones.*

Illustratively spoken, the benefit of this approach is that there are no discontinuities inside control volumes. Although the models are of comparatively low order the dynamic behaviour of evaporators and condensers can be described with high accuracy [1]. Special attention has to be paid to the cases, when phase boundaries are disappearing and therefore control volumes disappear.

Moving boundary heat exchanger models can be found in many control related publications [2, 3, 4, 5, 6]. Usually the derived DAE system is given in descriptor form. Modelica as an object-oriented equation based modeling languages provides the possibility to formulate models in a highly reusable and natural way [7]. The symbolic transformation into a numerical suitable form is done by a simulation tool. To the authors' best knowledge there are only two publications about moving boundary models written in Modelica [8, 9] or other equation based languages. In this work the thermodynamically exact derivation of moving boundary models for condensers and evaporators is described. In contrast to models in previous literature the energy and mass balance equations are exactly fulfilled. Additionally, there are no unphysical equations needed as they are added in many moving-boundary models in order to get stable switching behaviour [4, 5].

Existing publications with experimental validation of moving-boundary models usually examine a whole vapour compression cycle. We propose a validation procedure that allows a deeper look inside the heat exchangers. In addition to temperatures, pressures and mass flow rates the length of the different zones (superheated, two-phase, subcooled) can be directly measured by high-speed infrared thermography. We show the feasibility of this method by analyzing an automotive condenser. The exact comparison of numerical and experimental data will be part of future work.

2 Moving Boundary Heat-Exchanger Model

In this section the derivation of the governing equations for different control volumes is presented. These equations are then used to build up an evaporator and a condenser model. Both models consist at maximum of three zones: subcooled, superheated and two-phase. The single-phase zones can dynamically appear and disappear. The switching of the different modes is a crucial part of the model. It is important to formulate these implicitly defined discontinuities in a way that no inconsistent switching occurs for all system states. This topic is handled in an extra subsection.

Tab. 1 *Symbols used in the model equations.*

Symbol	Unit	Description
α	$\frac{\mathrm{W}}{\mathrm{m}^2\,\mathrm{K}}$	Heat transfer coefficient
γ	-	Void fraction
μ	-	Density ratio
ρ	$\frac{\mathrm{kg}}{\mathrm{m}^3}$	Density
A	m^2	Area
c	$\frac{\mathrm{J}}{\mathrm{kg\,K}}$	Specific heat capacity
h	$\frac{\mathrm{J}}{\mathrm{kg}}$	Specific enthalpy
H	J	Total enthalpy
L	m	Total heat exchanger length
m	kg	Mass
$\dot{m}$	$\frac{\mathrm{kg}}{\mathrm{s}}$	Mass flow rate
p	Pa	Pressure
$\dot{Q}$	W	Heat flow rate
t	s	Time
T	K	Temperature
V	m^3	Volume
w	$\frac{m}{s}$	Velocity
x	-	Extended vapour quality
y	m	Zone length

2.1 General refrigerant equations

The basis for all above derived equations is mass and energy balances for an open control volume. As

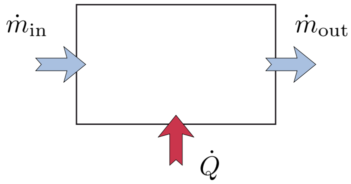

Fig. 2 *Refrigerant control volume*

sketched in Fig. 2 there is one fluid flow entering and one leaving the control volume leading to the mass balance:

$$\frac{\mathrm{d}m}{\mathrm{d}t} = \dot{m}_{\mathrm{in}} - \dot{m}_{\mathrm{out}}. \tag{1}$$

Negelecting kinetic and potential energy the energy balance can be stated as

$$\frac{\mathrm{d}H}{\mathrm{d}t} = \dot{m}_{\mathrm{in}}h_{\mathrm{in}} - \dot{m}_{\mathrm{out}}h_{\mathrm{out}} + \dot{Q} + \frac{\mathrm{d}p}{\mathrm{d}t}A_{\mathrm{c}}y, \tag{2}$$

where y is the control volume length and A_{c} the cross sectional area. With $H = mh$ and Eq. (1) the energy balance can also be formulated as

$$\begin{aligned} m\frac{\mathrm{d}h}{\mathrm{d}t} = \dot{m}_{\mathrm{in}}(h_{\mathrm{in}} - h) - \dot{m}_{\mathrm{out}}(h_{\mathrm{out}} - h) \\ + \dot{Q} + \frac{\mathrm{d}p}{\mathrm{d}t}A_{\mathrm{c}}y. \end{aligned} \tag{3}$$

2.2 Refrigerant single phase equations

For single phase flow a linear enthalpy distribution inside the control volume is assumed. The mean enthalpy h can be calculated out of the boundary enthalpies:

$$h = \frac{h_{\mathrm{A}} + h_{\mathrm{B}}}{2}. \tag{4}$$

Density can be expressed as a function of pressure and enthalpy:

$$\rho = \rho(p,\, h). \tag{5}$$

The refrigerant mass is

$$m = \rho A_{\mathrm{c}} y. \tag{6}$$

Inserted into the general mass balance Eq. (1) it becomes

$$\frac{\mathrm{d}\rho}{\mathrm{d}t}A_{\mathrm{c}}y + \frac{\mathrm{d}y}{\mathrm{d}t}\rho A_{\mathrm{c}} = \dot{m}_{\mathrm{in}} - \dot{m}_{\mathrm{out}}, \tag{7}$$

with

$$\frac{\mathrm{d}\rho}{\mathrm{d}t} = \left(\frac{\partial \rho}{\partial p}\right)_h \frac{\mathrm{d}p}{\mathrm{d}t} + \left(\frac{\partial \rho}{\partial h}\right)_p \frac{\mathrm{d}h}{\mathrm{d}t}. \tag{8}$$

Eq. (8) is derived by differentiating Eq. (5). The partial derivatives are fluid properties and can be calculated as functions of p and h.

For single phase flow the energy balance Eq. (3) is considered. Additional equations are required to determine the heat flow rate entering the control volume.

2.3 Refrigerant two phase equations

For two phase flow an important variable is the volumetric void fraction γ which is defined as

$$\gamma = \frac{V_{\mathrm{d}}}{V_{\mathrm{d}} + V_{\mathrm{b}}}, \tag{9}$$

where V_{d} is the total vapour volume and V_{b} the total liquid volume inside the control volume. The indices stand for dew and bubble. With this definition the total refrigerant mass can be calculated out of the liquid and vapour densities:

$$m = A_{\mathrm{c}}y\,(\gamma\rho_{\mathrm{d}} + (1-\gamma)\rho_{\mathrm{b}}). \tag{10}$$

Differentiating Eq. (10) and inserting it into the general mass balance Eq. (1) leads to

$$\begin{aligned} \frac{\mathrm{d}y}{\mathrm{d}t}A_{\mathrm{c}}(\gamma\rho_{\mathrm{d}} + (1-\gamma)\rho_{\mathrm{b}}) + yA_{\mathrm{c}}\Bigg(\frac{\mathrm{d}\gamma}{\mathrm{d}t}(\rho_{\mathrm{d}} - \rho_{\mathrm{b}}) \\ + \gamma\frac{\mathrm{d}\rho_{\mathrm{d}}}{\mathrm{d}t} + (1-\gamma)\frac{\mathrm{d}\rho_{\mathrm{b}}}{\mathrm{d}t}\Bigg) = \dot{m}_{\mathrm{in}} - \dot{m}_{\mathrm{out}}. \end{aligned} \tag{11}$$

Similar to the total mass in Eq. (10) we can formulate the total enthalpy as weighted sum of liquid and vapour enthalpy:

$$H = yA_{\mathrm{c}}\left(\gamma\rho_{\mathrm{d}}h_{\mathrm{d}} + (1-\gamma)\rho_{\mathrm{b}}h_{\mathrm{b}}\right). \tag{12}$$

To obtain the two phase energy balance formulation, Eq. (12) is differentiated and combined with the general energy balance Eq. (2):

$$\begin{aligned} \frac{\mathrm{d}y}{\mathrm{d}t}A_{\mathrm{c}}\left(\gamma\rho_{\mathrm{d}}h_{\mathrm{d}} + (1-\gamma)\rho_{\mathrm{b}}h_{\mathrm{b}}\right) \\ + yA_{\mathrm{c}}\Bigg(\frac{\mathrm{d}\gamma}{\mathrm{d}t}(\rho_{\mathrm{d}}h_{\mathrm{d}} - \rho_{\mathrm{b}}h_{\mathrm{b}}) \\ + \gamma\frac{\mathrm{d}(\rho_{\mathrm{d}}h_{\mathrm{d}})}{\mathrm{d}t} + (1-\gamma)\frac{\mathrm{d}(\rho_{\mathrm{b}}h_{\mathrm{b}})}{\mathrm{d}t}\Bigg) \\ = \dot{m}_{\mathrm{in}}h_{\mathrm{in}} - \dot{m}_{\mathrm{out}}h_{\mathrm{out}} + \dot{Q} + \frac{\mathrm{d}p}{\mathrm{d}t}A_{\mathrm{c}}y. \end{aligned} \tag{13}$$

The total derivatives of thermodynamic state variables on the dew and bubble curve as they occur in Eq. (11)

and Eq. (13) can be calculated according to the following derivation. As example we take the density on the dew curve ρ_d. The same principles hold for all other state variables, too. In general density can be expressed as function of pressure and temperature. On the dew curve temperature itself is not independent but a function of pressure, given by the saturation curve:

$$\rho_\mathrm{d} = \rho(p, T_\mathrm{s}(p)). \tag{14}$$

Differentiating this equation leads to

$$\frac{\mathrm{d}\rho_\mathrm{d}}{\mathrm{d}t} = \left(\frac{\partial \rho}{\partial p}\right)_T \frac{\mathrm{d}p}{\mathrm{d}t} + \left(\frac{\partial \rho}{\partial T}\right)_p \frac{\mathrm{d}T_\mathrm{s}}{\mathrm{d}p}\frac{\mathrm{d}p}{\mathrm{d}t}. \tag{15}$$

The remaining partial derivatives, as well as the derivative of the saturation curve are fluid properties.

To complete the set of equations we have to take care of one more unknown: the void ratio γ. Void ratio is not constant along the direction of flow. The total volumetric void fraction is actually a mean value of the local void fraction γ':

$$\gamma = \frac{1}{y}\int_0^y \gamma'(\tilde{y})\,\mathrm{d}\tilde{y}. \tag{16}$$

There exists a variety of mathematical models to describe the local void fraction. Thome [10] gives an excellent introduction to this topic. In this work we use the well-known model of Zivi [11]:

$$\gamma'(\tilde{y}) = \frac{1}{1 + \frac{1-x(\tilde{y})}{x(\tilde{y})}\left(\frac{\rho_\mathrm{d}}{\rho_\mathrm{b}}\right)^{2/3}}, \tag{17}$$

where x is the local vapour mass fraction. The density ratio $\mu := \frac{\rho_\mathrm{d}}{\rho_\mathrm{b}}$ is only a function of pressure and is constant along the direction of flow. We insert Eq. (17) into Eq. (16) and integrate analytically assuming that x is linear in $\tilde{y}$. The result is

$$\gamma = \frac{(x_\mathrm{B}-x_\mathrm{A})(1-\mu^{2/3})^2 + \mu^{2/3}\ln\frac{x_\mathrm{A}(\mu^{-2/3}-1)+1}{x_\mathrm{B}(\mu^{-2/3}-1)+1}}{(x_\mathrm{B}-x_\mathrm{A})(\mu^{2/3}-1)^2}, \tag{18}$$

where x_A denotes the vapour mass fraction at $\tilde{y} = 0$ and x_B at $\tilde{y} = y$. For the mass and energy balance equations we need the total derivative of γ, which can be obtained by differentiating Eq. (18):

$$\begin{aligned}\frac{\mathrm{d}\gamma}{\mathrm{d}t} = \left(\frac{\partial\gamma}{\partial x_\mathrm{A}}\right)_{x_\mathrm{B},\mu}\frac{\mathrm{d}x_\mathrm{A}}{\mathrm{d}t} + \left(\frac{\partial\gamma}{\partial x_\mathrm{B}}\right)_{x_\mathrm{A},\mu}\frac{\mathrm{d}x_\mathrm{B}}{\mathrm{d}t}\\ + \left(\frac{\partial\gamma}{\partial\mu}\right)_{x_\mathrm{A},x_\mathrm{B}}\frac{\mathrm{d}\mu}{\mathrm{d}p}\frac{\mathrm{d}p}{\mathrm{d}t}\end{aligned} \tag{19}$$

Analytical expressions for the partial derivatives can be derived from Eq. (18). The total derivative of the density ratio is a fluid property. The total derivatives of the inlet and outlet vapour mass fractions depend on the heat exchangers state. They are equal zero if all three zones exist.

2.4 Wall material equations

The wall material of every zone is a separate control volume. Solid density ρ and specific heat capacity c is assumed as constant. The temperature is time dependent but equally distributed. Treating the wall material as thermodynamic phase the variable control volume boundary can be associated with an enthalpy flow that enters or leaves the control volume. The energy balance is

$$m\frac{\mathrm{d}h}{\mathrm{d}t} = \dot{m}_\mathrm{A}(h_\mathrm{A}-h) + \dot{m}_\mathrm{B}(h_\mathrm{B}-h) - \dot{Q}_\mathrm{i} + \dot{Q}_\mathrm{o}. \tag{20}$$

The specfic enthalpy can be expressed as $h = c(T - T_0)$ leading to

$$mc\frac{\mathrm{d}T}{\mathrm{d}t} = \dot{m}_\mathrm{A}c(T_\mathrm{A}-T) + \dot{m}_\mathrm{B}c(T_\mathrm{B}-T) - \dot{Q}_\mathrm{i} + \dot{Q}_\mathrm{o}. \tag{21}$$

We introduce two new variables, w_A and w_B, which denote the velocities of the zone boundaries. Both variables are defined to be positive if the boundary movement corresponds to a growing control volume. The boundary wall temperatures depend on the boundary's movement direction:

$$T_\mathrm{A} = \begin{cases} T & \text{if} \quad w_\mathrm{A} \le 0 \\ T_\mathrm{A}^+ & \text{if} \quad w_\mathrm{A} > 0 \end{cases}, \tag{22}$$

$$T_\mathrm{B} = \begin{cases} T & \text{if} \quad w_\mathrm{B} \le 0 \\ T_\mathrm{B}^+ & \text{if} \quad w_\mathrm{B} > 0 \end{cases}. \tag{23}$$

T_A^+ and T_B^+ denote the wall temperatures of the neighbouring zones. Finally we introduce the wall's cross sectional area A_w and write:

$$\begin{aligned}\rho A_\mathrm{w} c\frac{\mathrm{d}T}{\mathrm{d}t} = \rho A_\mathrm{w} w_\mathrm{A} c(T_\mathrm{A}-T)\\ +\rho A_\mathrm{w} w_\mathrm{B} c(T_\mathrm{B}-T) - \dot{Q}_\mathrm{i} + \dot{Q}_\mathrm{o}.\end{aligned} \tag{24}$$

2.5 Evaporator model

The evaporator model consists of maximum three zones: subcooled (index 1), two-phase (index 2) and superheated (index 3). Zones 1 and 3 can dynamically disappear and appear. The corresponding switching conditions are discussed in section 2.8. The resulting differential state vector is:

$$x_{\mathrm{evp}} := (p, y_2, y_3, h_{\mathrm{out}}, T_{\mathrm{w},1}, T_{\mathrm{w},2}, T_{\mathrm{w},3}). \tag{25}$$

Input variables, which have to be provided from other models or boundary conditions, are:

$$u_{\mathrm{evp}} := (\dot{m}_{\mathrm{in}}, \dot{m}_{\mathrm{out}}, h_{\mathrm{in}}, \frac{\mathrm{d}h_{\mathrm{in}}}{\mathrm{d}t}). \tag{26}$$

2.5.1 Refrigerant mass balance equations

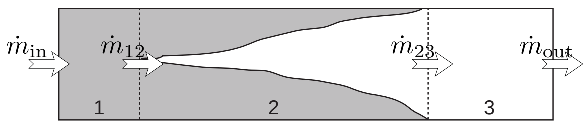

Fig. 3 *Evaporator zones and mass flow rates.*

The total heat exchanger length L is equal to the sum of all zone lengths:

$$y_1 + y_2 + y_3 = L \Rightarrow \frac{\mathrm{d}y_1}{\mathrm{d}t} = -\frac{\mathrm{d}y_2}{\mathrm{d}t} - \frac{\mathrm{d}y_3}{\mathrm{d}t}. \tag{27}$$

The mass balance for the subccoled zone is

$$\begin{aligned} \dot{m}_{\mathrm{in}} - \dot{m}_{12} = A_{\mathrm{c}} \Bigg[\left(-\frac{\mathrm{d}y_2}{\mathrm{d}t} - \frac{\mathrm{d}y_3}{\mathrm{d}t} \right) \rho_1 \\ + \frac{\mathrm{d}p}{\mathrm{d}t} y_1 \left(\left(\frac{\partial \rho_1}{\partial p} \right)_{h_1} + \frac{1}{2} \left(\frac{\partial \rho_1}{\partial h_1} \right)_p \frac{\mathrm{d}h_{\mathrm{b}}}{\mathrm{d}p} \right) \\ + \frac{\mathrm{d}h_{\mathrm{in}}}{\mathrm{d}t} \frac{y_1}{2} \left(\frac{\partial \rho_1}{\partial h_1} \right)_p \Bigg], \end{aligned} \tag{28}$$

for the two-phase zone

$$\begin{aligned} \dot{m}_{12} - \dot{m}_{23} = A_{\mathrm{c}} \Bigg[\frac{\mathrm{d}y_2}{\mathrm{d}t} \left(\gamma \rho_{\mathrm{d}} + (1-\gamma) \rho_{\mathrm{b}} \right) \\ + \frac{\mathrm{d}\gamma}{\mathrm{d}t} y_2 \left(\rho_{\mathrm{d}} - \rho_b \right) \\ + \frac{\mathrm{d}p}{\mathrm{d}t} y_2 \left(\gamma \frac{\mathrm{d}\rho_{\mathrm{d}}}{\mathrm{d}p} + (1-\gamma) \frac{\mathrm{d}\rho_{\mathrm{b}}}{\mathrm{d}p} \right) \Bigg], \end{aligned} \tag{29}$$

and finally for the superheated zone

$$\begin{aligned} \dot{m}_{23} - \dot{m}_{\mathrm{out}} = A_{\mathrm{c}} \Bigg[\frac{\mathrm{d}y_3}{\mathrm{d}t} \rho_3 \\ + \frac{\mathrm{d}p}{\mathrm{d}t} y_3 \left(\left(\frac{\partial \rho_3}{\partial p} \right)_{h_3} + \frac{1}{2} \left(\frac{\partial \rho_3}{\partial h_3} \right)_p \frac{\mathrm{d}h_{\mathrm{d}}}{\mathrm{d}p} \right) \\ + \frac{\mathrm{d}h_{\mathrm{out}}}{\mathrm{d}t} \frac{y_3}{2} \left(\frac{\partial \rho_3}{\partial h_3} \right)_p \Bigg]. \end{aligned} \tag{30}$$

2.5.2 Refrigerant energy balance equations

The energy balance for the subcooled zone is

$$\begin{aligned} A_{\mathrm{c}} \left[\frac{\mathrm{d}p}{\mathrm{d}t} y_1 \left(\frac{\rho_1}{2} \frac{\mathrm{d}h_{\mathrm{b}}}{\mathrm{d}p} - 1 \right) + \frac{\mathrm{d}h_{\mathrm{in}}}{\mathrm{d}t} y_1 \frac{\rho_1}{2} \right] \\ = \dot{m}_{\mathrm{in}} \left(h_{\mathrm{in}} - h_1 \right) - \dot{m}_{12} \left(h_{\mathrm{b}} - h_1 \right) + \dot{Q}_{\mathrm{i},1}, \end{aligned} \tag{31}$$

for the two-phase zone

$$\begin{aligned} A_{\mathrm{c}} \Bigg[\frac{\mathrm{d}y_2}{\mathrm{d}t} \left(\gamma \rho_{\mathrm{d}} h_{\mathrm{d}} + (1-\gamma) \rho_{\mathrm{b}} h_{\mathrm{b}} \right) \\ + \frac{\mathrm{d}\gamma}{\mathrm{d}t} y_2 \left(\rho_{\mathrm{d}} h_{\mathrm{d}} - \rho_{\mathrm{b}} h_{\mathrm{b}} \right) \\ \frac{\mathrm{d}p}{\mathrm{d}t} y_2 \left(\gamma \frac{\mathrm{d}(\rho_{\mathrm{d}} h_{\mathrm{d}})}{\mathrm{d}p} + (1-\gamma) \frac{\mathrm{d}(\rho_{\mathrm{b}} h_{\mathrm{b}})}{\mathrm{d}p} - 1 \right) \Bigg] \\ = \dot{m}_{12} h_{12} - \dot{m}_{23} h_{23} + \dot{Q}_{\mathrm{i},2}, \end{aligned} \tag{32}$$

and finally for the superheated zone

$$\begin{aligned} A_{\mathrm{c}} \left[\frac{\mathrm{d}p}{\mathrm{d}t} y_3 \left(\frac{\rho_3}{2} \frac{\mathrm{d}h_{\mathrm{d}}}{\mathrm{d}p} - 1 \right) + \frac{\mathrm{d}h_{\mathrm{out}}}{\mathrm{d}t} y_3 \frac{\rho_3}{2} \right] \\ = \dot{m}_{23} \left(h_{23} - h_3 \right) - \dot{m}_{\mathrm{out}} \left(h_{\mathrm{out}} - h_3 \right) + \dot{Q}_{\mathrm{i},3}. \end{aligned} \tag{33}$$

2.6 Condenser model

The condenser model consists of maximum three zones: superheated (index 1), two-phase (index 2) and subcooled (index 3). Zones 1 and 3 can dynamically disappear and appear. The corresponding switching conditions are discussed in section 2.8. The resulting differential state vector is:

$$x_{\mathrm{cond}} := (p, y_1, y_2, h_{\mathrm{out}}, T_{\mathrm{w},1}, T_{\mathrm{w},2}, T_{\mathrm{w},3}). \tag{34}$$

Input variables, which have to be provided from other models or boundary conditions, are:

$$u_{\mathrm{cond}} := (\dot{m}_{\mathrm{in}}, \dot{m}_{\mathrm{out}}, h_{\mathrm{in}}, \frac{\mathrm{d}h_{\mathrm{in}}}{\mathrm{d}t}). \tag{35}$$

2.6.1 Mass balance equations

The total heat exchanger length L is equal to the sum of all zone lengths:

$$y_1 + y_2 + y_3 = L \Rightarrow \frac{\mathrm{d}y_3}{\mathrm{d}t} = -\frac{\mathrm{d}y_1}{\mathrm{d}t} - \frac{\mathrm{d}y_2}{\mathrm{d}t}. \tag{36}$$

The mass balance for the superheated zone is

$$\dot{m}_{\mathrm{in}} - \dot{m}_{12} = A_{\mathrm{c}} \Bigg[\frac{\mathrm{d}y_1}{\mathrm{d}t} \rho_1 + \frac{\mathrm{d}p}{\mathrm{d}t} y_1 \left(\left(\frac{\partial \rho_1}{\partial p} \right)_{h_1} + \frac{1}{2} \left(\frac{\partial \rho_1}{\partial h_1} \right)_p \frac{\mathrm{d}h_{\mathrm{d}}}{\mathrm{d}p} \right) + \frac{\mathrm{d}h_{\mathrm{in}}}{\mathrm{d}t} \frac{y_1}{2} \left(\frac{\partial \rho_1}{\partial h_1} \right)_p \Bigg]. \tag{37}$$

Two-phase zone's mass balance is identical to Eq. (29). For the subcooled zone it is

$$\dot{m}_{23} - \dot{m}_{\mathrm{out}} = A_{\mathrm{c}} \Bigg[\left(-\frac{\mathrm{d}y_1}{\mathrm{d}t} - \frac{\mathrm{d}y_2}{\mathrm{d}t} \right) \rho_3 + \frac{\mathrm{d}p}{\mathrm{d}t} y_3 \left(\left(\frac{\partial \rho_3}{\partial p} \right)_{h_3} + \frac{1}{2} \left(\frac{\partial \rho_3}{\partial h_3} \right)_p \frac{\mathrm{d}h_{\mathrm{b}}}{\mathrm{d}p} \right) + \frac{\mathrm{d}h_{\mathrm{out}}}{\mathrm{d}t} \frac{y_3}{2} \left(\frac{\partial \rho_3}{\partial h_3} \right)_p \Bigg]. \tag{38}$$

2.6.2 Energy balance equations

The energy balance for the superheated zone is

$$A_{\mathrm{c}} \left[\frac{\mathrm{d}p}{\mathrm{d}t} y_1 \left(\frac{\rho_1}{2} \frac{\mathrm{d}h_{\mathrm{d}}}{\mathrm{d}p} - 1 \right) + \frac{\mathrm{d}h_{\mathrm{in}}}{\mathrm{d}t} y_1 \frac{\rho_1}{2} \right] = \dot{m}_{\mathrm{in}} \left(h_{\mathrm{in}} - h_1 \right) - \dot{m}_{12} \left(h_{\mathrm{d}} - h_1 \right) + \dot{Q}_{\mathrm{i},1}. \tag{39}$$

Two-phase zone's energy balance is identical to Eq. (32). For the subcooled zone it is

$$A_{\mathrm{c}} \left[\frac{\mathrm{d}p}{\mathrm{d}t} y_3 \left(\frac{\rho_3}{2} \frac{\mathrm{d}h_{\mathrm{b}}}{\mathrm{d}p} - 1 \right) + \frac{\mathrm{d}h_{\mathrm{out}}}{\mathrm{d}t} y_3 \frac{\rho_3}{2} \right] = \dot{m}_{23} \left(h_{23} - h_3 \right) - \dot{m}_{\mathrm{out}} \left(h_{\mathrm{out}} - h_3 \right) + \dot{Q}_{\mathrm{i},3}. \tag{40}$$

2.7 Additional equations

For both models, evaporator and condenser, there are three additional energy balance equations for the wall volume of each zone. These are derived from Eq. (22), Eq. (23) and Eq. (24). Furthermore we need equations to calculate the heat flow rates. The inner heat flow rate

$$\dot{Q}_{\mathrm{i,n}} = \alpha_{\mathrm{i,n}} y_{\mathrm{n}} A'_{\mathrm{i}} (T_{\mathrm{w,n}} - T_{\mathrm{n}}), \tag{41}$$

where A'_{i} is the inner heat transfer area per length. $\alpha_{\mathrm{i,n}}$ is the heat transfer coefficient, which is in general not equal for all zones n. This is important because its value is much different for two-phase and one-phase flow.

The outer heat flow rate depends on the secondary medium and the heat exchanger design. In our example we have chosen a cross flow MPET heat exchangers and air as secondary medium. We assume that α_{o} is equal for all zones:

$$\dot{Q}_{\mathrm{o,n}} = \alpha_{\mathrm{o}} y_{\mathrm{n}} A'_{\mathrm{o}} (T_{\mathrm{air}} - T_{\mathrm{w,n}}). \tag{42}$$

The moving boundary heat exchanger models are integrated into the object-oriented framework of the Modelica library TIL [12, 13], allowing a user-friendly detailed geometrical parameterisation for different heat exchanger types. Sophisticated heat transfer correlations for the refrigerant as well as the air side can be used.

2.8 Switching model representation

A crucial part of general moving boundary models is the switching between different number of active zones. There exist various more or less complex switching conditions in literature. We propose a new switching condition, which depends only on one variable. In this section we focus on the condenser model. The same basic principles also hold for the evaporator model.

The subcooled and the superheated zone of the condenser model can become zero. In order to detect the switching between different modes an extended vapour quality at the inlet and outlet is introduced:

$$x_{\mathrm{in}} = \frac{h_{\mathrm{in}} - h_{\mathrm{b}}}{h_{\mathrm{d}} - h_{\mathrm{b}}} \tag{43a}$$

$$x_{\mathrm{out}} = \frac{h_{\mathrm{out}} - h_{\mathrm{b}}}{h_{\mathrm{d}} - h_{\mathrm{b}}} \tag{43b}$$

In the two-phase region its value is between 0 and 1 and is equal to the mass fraction of saturated vapour to the total mass. Outside the two-phase region values higher than 1 indicate superheated states and values lower than 0 indicate subcooled states. In other words, there is a subcooled zone if $x_{\mathrm{out}} < 0$ and there is a superheated zone if $x_{\mathrm{in}} > 1$. These are exactly the switching conditions in the model. The corresponding Modelica code for the superheated zone is:

```
if (x_in > 1.0) then
  h_12 = h_d;
  A_c * (der(y1) * ref1.d
  + der(p) * max(y1, 1e-8)
  * (ref1.drhodp + ref1.drhodh/2
  * dhdp_d) + der(h_in)
 * max(y1, 1e-8) * ref1.drhodh/2)
  = mdot_in - mdot_12;
  /* mass balance Eq. (37) */
  A_c * (der(p) * max(y1, 1e-8)
  * (ref1.d / 2 * dhdp_d - 1)
  + der(h_in) * max(y1, 1e-8) * ref1.d/2)
  = mdot_in * (h_in - ref1.h)
  - mdot_12 * (h_12 - ref1.h) + Qdot1;
```

/* energy balance Eq. (39) */

```
else

  h_12 = h_in;

  der(y1) = 0.0;
  mdot_12 = mdot_in;

end if;
```

In the `ref1` object the fluid property calculations are located. Its classs is `TILMedia.Refrigerant` out of the object oriented fluid property Library TILMedia [12, 13]. For the subcooled zone we get a similar Modelica code:

```
if (x_out < 0.0) then

  h_23 = h_b;

  A_c * (ref3.d * (-der(y1)-der(y2))
  + der(p) * max(y3,1e-8)
  * (ref3.drhodp + ref3.drhodh/2
  * dhdp_b) + der(h_out)
  * max(y3,1e-8) * ref3.drhodh/2)
  = mdot_23 - mdot_out;
```

/* mass balance Eq. (38) */

```
  A_c * (der(p) * max(y3,1e-8)
  * (ref3.d/2 * dhdp_b - 1)
  + der(h_out) * max(y3,1e-8)
  * ref3.d/2)
  = mdot_23 * (h_23 - ref3.h)
  - mdot_out * (h_out  - ref3.h) + Qdot3;
```

/* energy balance Eq. (40) */

```
else

  h_12 = h_in;

  der(y2) + der(y3) = 0.0;
  mdot_12 = mdot_in;

end if;
```

Translating this set of hybrid differential and algebraic equations with the Modelica tool Dymola leads to a system of equations which is linear in the state derivatives:

$$A(x_{\text{cond}}, u_{\text{cond}})\dot{x}_{\text{cond}} = b(x_{\text{cond}}, u_{\text{cond}}). \qquad (44)$$

The matrix and vector elements of A and b are nonlinear and include the discontinuities introduced with the above derived if equations. Additional balance equations for the air-side and heat transfer correlations lead to a hybrid DAE of index one.

To understand what happens when we approach a switching point during simulation we look at the switching from three to two zones, when the subcooling zone disappears. This is also the case in the simulation study in section 4. When the outlet vapour quality x_{out} crosses zero an event is triggered and the integration is restarted with different values in A and b. It is important to notice that the zone length y_3 also approaches zero as expected. This is only the result of thermodynamically consistent balance and fluid property equations. Numerical errors during integration and errors in the fluid property calculation lead to the fact, that y_3 ist not perfectly equal zero when $x_{\text{out}} = 0$ but has a small nonzero value which can also be negative. Negative values of zone lengths are physically unfeasible and lead to an unstable behaviour of the ODE Eq. (44). On the other hand zone lengths at exactly zero lead to a singular Matrix A. Therefore we protect the model against values of y_1 and y_3 below a small positive number. As one can see in the code example above this is realised by the Modelica `max()` operator.

3 Validation Procedure

Properly designed validation experiments are necessary to establish a satisfactory level confidence in simulation models. In terms of the moving boundary heat exchanger model described above knowledge on the location of superheating- and subcooling-fronts is the major information needed for validation. Therefore a measurement procedure allowing determination of these fronts under transient conditions is needed. One possibility to determine the location of these fronts is measurement of wall temperature. Infrared thermography allows for high resolution measurement of wall temperatures both in terms of spatial and time coordinate.

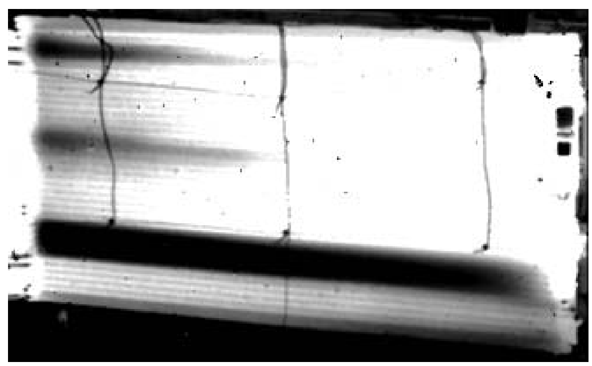

(a) *1st pass with de-superheating and condensing, 2nd pass no subcooling.*

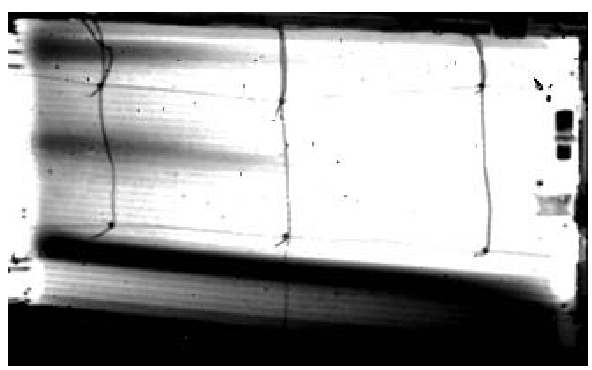

(b) *1st pass with de-superheating and condensing, 2nd: condensing and subcooling.*

Fig. 4 *Thermograms depicting an automotive condenser with two passes.*

In recent years, a number of studies have been published on infrared thermography in heat transfer and flow visualization. Simeonides et al. [14] and Henckels et al. [15] developed the infrared thermographic technique in the measurement of heat transfer in a hypersonic wind tunnel. This technique was applied to determine local heat transfer in heat exchangers e.g. by Ay et al. [16]. Most studies focus on local phenomena rather than looking at the heat exchanger in total. Therefore tracking of subcooling- and superheating-fronts by thermography have so far only been published for single tubes and not total heat exchangers (e.g. [17]).

Fig. 4 depicts two exemplary thermograms of an automotive condenser. As thermograms display the amount of infrared energy emitted, transmitted, and reflected by an object, brighter Regions indicate a high temperature while darker regions indicate a lower temperature. The condenser consists out of two passes. The refrigerant enters the first pass at the upper right, flows to the left, is redirected through intergrated receiver, enters the second pass and flows back to the right. In the upper thermogram only de-superheating and condensing takes place. The former only in the first pass, the second pass at the bottom is entirely white. This is different for the lower thermogram; the refrigeration cycle charge is high enough to establish subcooling in the second pass. The starting point of the subcooling area can be seen in the thermogram as a transition from white to dark. The location of this transition line is tracked using the Matlab Image Processing Toolbox.

4 Numerical Results

In this section we present simulation results of an example system. In Fig. 5 the graphical model set up is shown. The system consists of a cross-flow condenser with boundary conditions. On the air-side constant mass flow rate, pressure and inlet temperature are given. On the refrigerant-side inlet enthalpy is constant. The mass flow rates are given by two PT_1-blocks with different time constants.

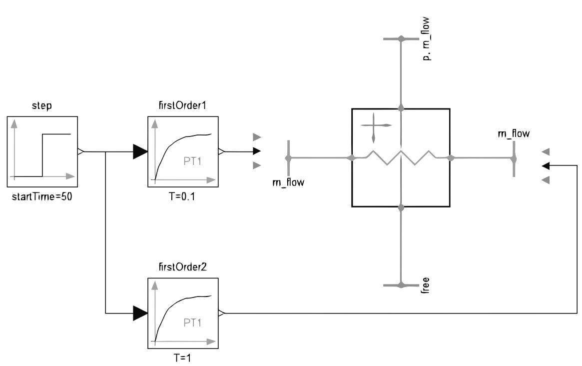

Fig. 5 *Graphical representation of the system model.*

During the first 50 seconds inlet and outlet mass flow rate are equal. At $t = 50\mathrm{s}$ a step jump is applied to the PT_1-blocks' inputs. Due to the larger time constant the outlet mass flow rate lags behind. After some time both mass flow rate are equal again. This changing boundary conditions cause a accumulation of refrigerant mass in the condenser. The corresponding trajectory is shown in Fig. 6.

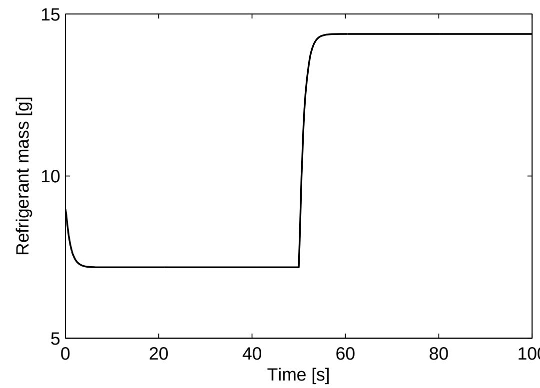

Fig. 6 *Trajectory of stored refrigerant mass in the condenser.*

As one can see in Fig. 7 the pressure, which is a differential state, also increases.

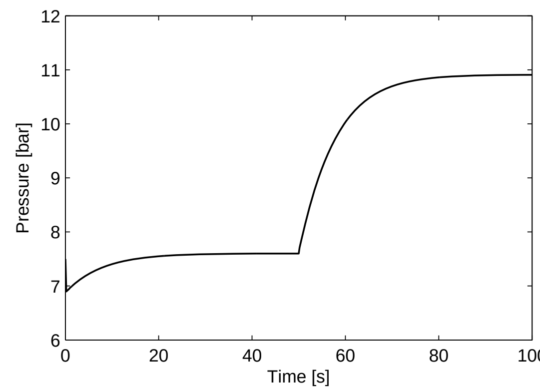

Fig. 7 *Trajectory of refrigerant pressure.*

In Fig. 8 the trajectory of the outlet vapour quality is shown. In the beginning we have values between 0 and 1. That means there is no subcooling. Shortly after the mass flow rate step jump we get values below 0 and after some time x_{out} gets positive again.

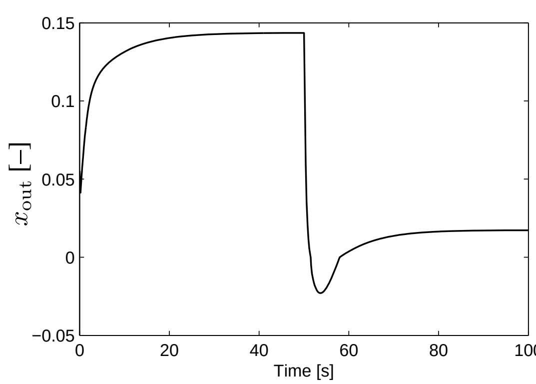

Fig. 8 *Trajectory of extended vapour quality at condenser's outlet.*

In Fig. 9 the trajectory of the relative zone lengths of the subcooled zone is shown. Reference value is the total condenser length. In the beginning the zone length is zero. We only have a superheated and a two-phase zone. When x_{out} gets 0 an event is triggered and the integration is restarted with different equations, as discussed in section 2.8. In this simulation result we actually see two switching events: one when the subcooled zone becomes active and one when it becomes inactive again.

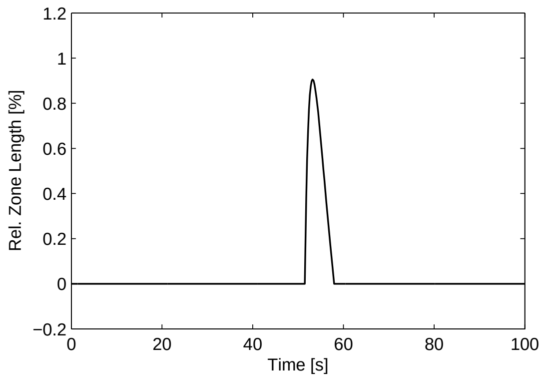

Fig. 9 *Trajectory of subcooled relative zone length.*

5 Conclusions

The object-oriented modeling language Modelica is well-suited for the formulation of moving boundary heat exchanger models as hybrid DAE. The thermodynamically exact derivation of the most important equations is shown in detail. An extended vapour mass fraction on the inlet and outlet is defined and used as switching condition. Numerical experiments show a robust behaviour of this new formulation. Additionally a new validation procedure is presented. Thermography allows detecting the phase boundary positions inside the heat exchanger. The actual validation of the models by this method will be part of future research. A specially designed test stand, which allows open loop experiments of heat exchangers, will be used.

6 References

[1] Satyam Bendapudi, James E. Braun, and Eckhard A. Groll. A comparison of moving-boundary and finite-volume formulations for transients in centrifugal chillers. *International Journal of Refrigeration*, 31(8):1437 – 1452, 2008.

[2] Brian D. Eldredge, Bryan P. Rasmussen, and Andrew G. Alleyne. Moving-boundary heat exchanger models with variable outlet phase. *Journal of Dynamic Systems, Measurement, and Control*, 130(6):061003, 2008.

[3] Bryan P. Rasmussen and Andrew G. Alleyne. Control-oriented modeling of transcritical vapor compression systems. *Journal of Dynamic Systems, Measurement, and Control*, 126(1):54–64, 2004.

[4] Thomas L. McKinley and Andrew G. Alleyne. An advanced nonlinear switched heat exchanger model for vapor compression cycles using the moving-boundary method. *International Journal of Refrigeration*, 31(7):1253 – 1264, 2008.

[5] Bin Li and Andrew G. Alleyne. A dynamic model of a vapor compression cycle with shut-down and start-up operations. *International Journal of Refrigeration*, 33(3):538 – 552, 2010.

[6] M. Willatzen, N.B.O.L. Pettit, and L. Ploug-Sørensen. A general dynamic simulation model for evaporators and condensers in refrigeration. part i: Moving-boundary formulation of two-phase flows with heat exchange. *International Journal of Refrigeration*, 21(5):398–403, 1998.

[7] Michael Tiller. *Introduction to Physical Modeling with Modelica*. Kluwer Academic Publishers, 2001.

[8] Wei-Jiang Zhang and Chun-Lu Zhang. A generalized moving-boundary model for transient simulation of dry-expansion evaporators under larger disturbances. *International Journal of Refrigeration*, 29(7):1119 – 1127, 2006.

[9] J. M. Jensen and H. Tummescheit. Moving boundary models for dynamic simulations of two-phase flows. In *Proceedings of the 2nd Int. Modelica Conference*, pages 235–244, Oberpfaffenhofen, Germany, 2002.

[10] John R. Thome. *Engineering Data Book III*. Wolverine Tube, Inc., 2009.

[11] S.M. Zivi. Estimation of steady-state steam void-fraction by means of the principle of minimum entropy production. *J. Heat Transfer*, 86:247–252, 1964.

[12] Christoph Richter. *Proposal of New Object-Oriented Equation-Based Model Libraries for Thermodynamic Systems*. PhD thesis, TU Braunschweig, 2008.

[13] M. Gräber, K. Kosowski, C. Richter, and W. Tegethoff. Modeling of heat pumps with an object-oriented model library for thermodynamic systems. In *Proceedings MATHMOD 09 Vienna*, 2009.

[14] G. Simeonides, P. Van Lierde, S. Van der Stichele, D. Capriotti, and J.F. Wendt. Infrared thermography in blowdown and intermittent hypersonic facilities. *Journal of Thermophysics and Heat Transfer*, 4(2):143–148, 1990.

[15] A. Henckels, F. Maurer, H. Olivier, and H. Grönig. Fast temperature measurement by infra-red line scanning in a hypersonic shock tunnel. *Experiments in Fluids*, 9(5):298–300, 1990.

[16] H. Ay, J. Jang, and J.-N. Yeh. Local heat transfer measurements of plate finned-tube heat exchangers by infrared thermography. *International Journal of Heat and Mass Transfer*, 45(20):4069–4078, 2002.

[17] M.C. Díaz and J. Schmidt. Experimental investigation of transient boiling heat transfer in microchannels. *International Journal of Heat and Fluid Flow*, 28(1 SPEC. ISS.):95–102, 2007.